Adaptive Cancellation of Parasitic Vibrations Affecting a Self-Mixing Interferometric Laser Sensor

Zohaib Ahmad Khan, Usman Zabit, Olivier Bernal, Muhammad M. Ullah, Thierry Bosch

Adaptive Cancellation of Parasitic Vibrations Affecting a Self-Mixing Interferometric Laser Sensor

ZohaibA. Khan, UsmanZabit, *Member*, *IEEE*, Olivier D. Bernal, *Member*, *IEEE*, Muhammad O. Ullah, *Member*, *IEEE*,andThierry Bosch,*Senior Member*, *IEEE*

***Abstract*—In this paper, an adaptive method of cancellation of parasitic vibrations is presented for a Self-Mixing (SM) interferometric laser vibration sensor which has been coupled with a solid state accelerometer (SSA). Previously, this was achieved by using a pre-calibration of phase and gain mismatches over the complete bandwidth of the instrument. Such a pre-calibration is not only tedious to execute but also hinders a mass production of the instrument as every SSA-SM sensor couple requires customized calibration. On the other hand, the proposed method does not require any pre-calibration as it uses an adaptive filter that self-tunes to match any unknown phase and gain differences between the SSA and the SM sensor. Two different adaptive algorithms, namely Recursive Least Squares (RLS) and Least Mean Squares (LMS) algorithms are tested and a comparison is established on the basis of parameter dependence, convergence time, computational cost and rms error. The proposed algorithms have provided improved results (mean error of 19.1nm and 20.2nm for LMS and RLS respectively) as compared to pre-calibration based results (mean error of 24.7 nm) for a laser wavelength of 785 nm. Simulated and experimental results thus demonstrate the utility of such an approach for embedded vibration sensing corrupted by extraneous parasitic motion.**

***Index Terms*—adaptive filter, self-mixing, vibration measurement, embedded sensing, optical feedback, laser instrument.**

I. Introduction

Self-mixing (SM) or optical feedback interferometry technique [1-3] is being actively researched for the measurement of displacement[4-5], distance [6], velocity [7], vibration [8], flow [9], profilometry [10], range-finding [11] and biomedical applications [12-13]due to the compact, self-aligned, and low-cost nature of the SM instrument.

These metric instruments have performed well in laboratory conditions. However, more work needs to be done so that these instruments can also be used for industrial and/or embedded applications, where extraneous/parasitic mechanical vibrations can disturb the measurement. In this regard, a solution consists in coupling a Solid-State Accelerometer (SSA) with a SM vibration sensor [14]. SSA then measures any extraneous/parasitic vibrations affecting the SM laser sensor. It then becomes possible to correct the corrupted measurement of SM sensor, even in real-time [15]. Such a scheme thus potentially enables the use of SM metric sensors for embedded/industrial applications.

However, it needs to be highlighted that the SSA-SM sensor required a pre-calibration of its full bandwidth before actual use [14]. Such a pre-calibration is mandatory in order to match the phase and gain differences between the SSA and the SM sensor. A phase and gain equalization filter was then designed in the light of the pre-calibration [14-15]. Otherwise, a correction of parasitic vibrations becomes ineffective.

This pre-calibration, done by mechanically shaking the SSA-SM sensor head over a whole range of frequencies covering its operating bandwidth, can pose four problems. First, it becomes tedious as well as cumbersome as each and every SSA-SM couple must mounted and shaken for its pre-calibration. This can then hinder a mass production of such an instrument. Second, the mechanical resonances affecting the shaker used for the pre-calibration can falsify the extraction of phase and gain parameters. Third, the phase and gain equalization filter would need to be individually designed for every SSA-SM couple. Consequently, any imprecision either in the extraction of phase and gain parameters or in the design of equalization filter causes added residual error. Fourthly, any subsequent mismatches due to aging or component change would necessitate a re-calibration of the instrument.

Therefore, in order to resolve all of these problems, in this paper, a method is proposed that enables cancellation of parasitic vibrations without needing any pre-calibration of the device. This is achieved by incorporating a self-tuning, adaptive filter. Two different adaptive algorithms have been tested, each providing different performance characteristics. The resulting sensor can thus adapt itself to the parasitic vibrations and provide corrected results after achieving convergence in an autonomous manner.

A schematic block diagram of the adaptive SSA-SM sensor is shown in Fig. 1. The SSA-SM sensor was mounted on a mechanical shaker (excited at different frequencies) in order to undergo parasitic vibrations, denoted as $D_s(t)$. A piezoelectric transducer (PZT) acted as a vibrating target as well as a reference sensor, denoted as $D_{PZT}(t)$. A photograph of the SSA-SM sensor can be seen in Fig. 2.

DOI: 10.1109/TIM.2016.2626018

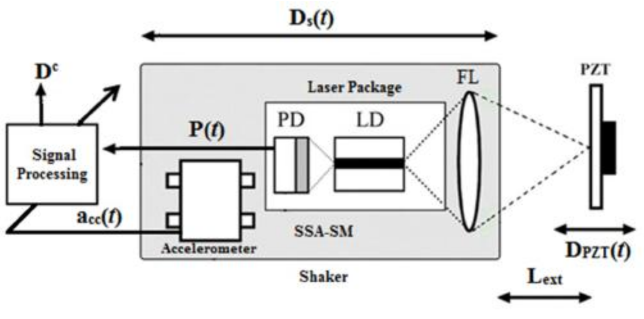

Fig. 1. Block diagram of the adaptive Solid-State Accelerometer coupled Self-Mixing (SSA-SM) sensor: photodiode (PD), laser diode (LD), focusing lens (FL), and piezoelectric transducer (PZT).

The paper is organized as follows. A brief introduction to SM interferometry is provided in section II. Then, the signal processing of the adaptive SSA-SM sensor is elaborated in section III. The simulated and experimental results are given in section IV, followed by the discussion and conclusion in Sections V and VI, respectively.

II. Self-Mixing Interferometry

The SM phenomenon happens in a laser when a part of the beam backscattered by a target is fed back into the active laser cavity, thereby causing interference with the emitted beam, which modifies the laser wavelength and output power. The variations in the optical output power $P(t)$ caused by this optical feedback can be written as [1]:

$$P(t) = P_0[1 + m.\cos(x_F(t))] \qquad (1)$$

Where P_0 is the emitted optical power under free-running conditions, m is the modulation index and $x_F(t)$ is the laser output phase in the presence of feedback, given by:

$$x_F(t) = 2\pi \frac{D(t)}{\lambda_F(t)/2} \qquad (2)$$

Where $D(t)$ is the target displacement.

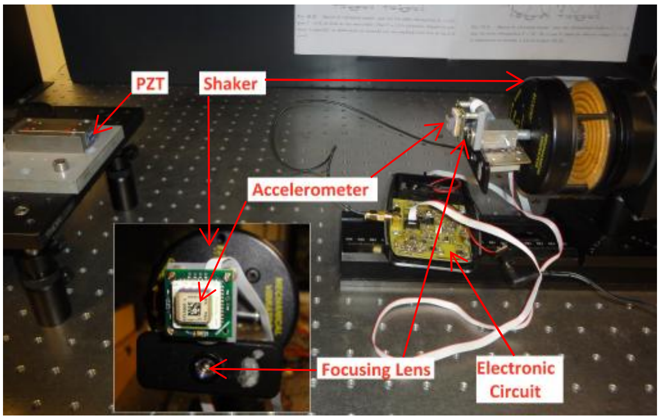

Fig. 2.Photograph of SSA-SM sensor using the SF1500 accelerometer and a SM displacement sensor based on DL7140 laser diode. The sensor head has been mounted on a mechanical shaker to undergo parasitic vibrations.

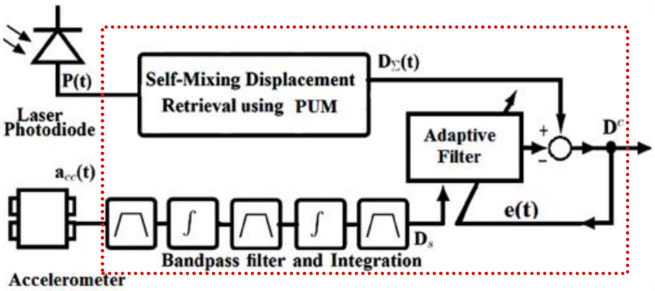

Fig. 3.Signal processing (shown in dotted red block) required for the adaptive SSA-SM sensor: PUM (Phase Unwrapping Method [23]).

Under optical feedback, $x_F(t)$ is determined by the well-established Lang-Kobayashi model [16], given as

$$x_0(t) - x_F(t) - C\sin[x_F(t) + \arctan(\alpha)] = 0 \qquad (3)$$

where α is the so called Henry's factor [17], also known as linewidth enhancement factor [18], C is the feedback coupling factor[19], also known as Acket's parameter [20-21] that determines the SM operating regime [22] and $x_0(t)$ is the laser output phase in the absence of feedback, found by replacing $\lambda_F(t)$ with λ in (2), where λ is the laser diode emission wavelength under free-running conditions.

III. Signal Processing

The signal processing of adaptive SSA-SM sensor (see Fig. 3) can be grouped in three major parts, as explained in the following.

A. *Self-mixing Interferometric Signal:*

The SM interferometric signal corresponds to the signal $P(t)$. Traditionally, $P(t)$ is easily acquired by using the built-in photodiode (PD) found inside the laser diode (LD) package (see Fig. 1). This SM interferometric signal can then be processed to recover the corresponding displacement or vibration signal. In this paper, we have used the Phase Unwrapping Method (PUM) offering a precision of λ/16 for displacement retrieval [23]. Note that for experimental SM signal acquisitions, the PUM automatically takes care of any variations in $P(t)$ caused by possible changes in system parameters, such as injection current, feedback strength, and target external cavity length, through the use of an automatic gain control stage [23].

Note that as shown in Fig. 3, the SM signal based measurement is denoted as $D_\Sigma(t)$ because it represents the sum of true target motion and parasitic motion i.e. $D_\Sigma(t)= D_{PZT}(t)+ D_s(t)$. It may be noted that it is assumed for the rest of this paper that the parasitic vibrations disturbing the SSA–SM sensor are of such an amplitude that the total motion does not influence the laser source and feedback based system parameters (e.g., C and α). It will be seen later in this paper that this assumption holds true for experimental SM signals acquired in the presence of parasitic vibrations.

B. *Acceleration Signal:*

As already mentioned, the extraneous vibration affecting the sensor (noted as $D_s(t)$) is measured by using a SSA. For this purpose, the acceleration signal $a_{cc}(t)$ is band-pass filtered

DOI: 10.1109/TIM.2016.2626018

and double-integrated (as shown in Fig. 3). The band-pass filtering is done so that low-frequency drifts that can cause offsets in the subsequent integration steps as well as high frequency acceleration signal saturation can be dealt with effectively.

C. *Adaptive Filter:*

An adaptive filter is a self-designing and time-varying system that continuously adapts/tunes its filter coefficients by following an adaptive algorithm with an aim of minimizing a cost/error function. Among other applications, such filters have been used for noise and echo cancellation [24].

In our case, the adaptive filter iteratively tunes itself by minimizing the mean square error (MSE) based on $e(t) = D_{\Sigma}(t) - D_s(t)$ (see Fig. 3). For statistically stationary inputs, the filter is said to have converged (i.e. tuned or designed) when it achieves the minimum MSE. Afterwards, it continues to perform its task (in our case, parasitic vibration cancellation) as long as the inputs retain their statistical nature. However, in case of change in the nature of inputs, the filter starts adapting itself to the new situation, and again achieves convergence to perform its task. For the present proof of concept, a transversal finite impulse response (FIR) adaptive filter structure has been evaluated using two different adaptive algorithms [least mean squares (LMS) and recursive least squares (RLS)] as detailed in the following.

1) Least Mean Square Algorithm (LMS): The LMS algorithm, known for its simplicity, stability, and robustness [24], belongs to the class of adaptive filters that adapts the filter coefficients by minimizing the MSE signal, where the error signal is the difference between the desired signal and the input signal, as defined below. In terms of adaptive filter terminology, the error $e(n)$ between the desired and weighted input signals is given by [24]

$$e(n) = d(n) - w^T X(n) \quad (4)$$

In our case, the corrupted signal $D_{\Sigma}(t)$ becomes desired signal $d(n)$and the parasitic signal $D_s(t)$ becomes input signal $X(n)$.

The filter coefficients in LMS algorithm are updated by:

$$w(n+1) = w(n) + 2\mu e(n)X(n) \quad (5)$$

For a given order of the filter N, the rate of convergence and filter's stability are determined by the step size (or convergence factor) denoted as μ, determined by

$$0 < \mu < \frac{1}{(N+1)P_{av}} \quad (6)$$

Where P_{av} is the average power of input signal $D_s(t)$. Thus, the LMS filter's stability and convergence rate become a function of average power of signal.

2) Recursive least square algorithm:

The Recursive Least Squares (RLS) adaptive algorithm recursively tunes the filter coefficients in order to minimize a weighted linear least squares cost function with respect to the input signal. The RLS algorithm is known for its excellent performance while working in time varying (non-stationary signals) environment but at the cost of an increased computational complexity and some stability problems [25].

RLS filter coefficients are updated by

$$w(n) = w(n-1) + k(n)e(n) \quad (7)$$

where k(n) is the filter gain given by

$$k(n) = \frac{\Lambda^{-1}\emptyset_{yy}(n-1)X(n)}{1+\Lambda^{-1}X^T(n)\emptyset_{yy}(n-1)X(n)} \quad (8)$$

Where Λ is the adaptation factor, and $\emptyset_{yy}$ is the correlation matrix, initially set to to identity matrix δI, and is recursively updated by.

$$\emptyset_{yy}(\text{n}) = \Lambda^{-1}\emptyset_{yy}(n-1) - \Lambda^{-1}k(n)X^T(n)\emptyset_{yy}(n-1) \quad (9)$$

Thus, the major difference between the LMS and RLS algorithms is the use of $\emptyset_{yy}$ in the correction term of the RLS algorithm which helps in achieving better convergence rate by decorrelating the successive inputs [25].

IV. RESULTS

A. *Experimental Setup*

The experimental set-up deployed for the validation of adaptive SSA-SM sensor has been schematized in Fig. 1. The employed SSA is a SF1500 accelerometer from Colibrys® (typical noise resolution of 0.3µg/Hz$^{1/2}$ and a full-scale range of ±3g). The SM sensor uses a Sanyo® DL7140 laser diode (λ=785 nm) with an output power of 50 mW. The SSA was glued on the SM sensor laser head so that it could measure as correctly as possible the parasitic movement $D_s(t)$ undergone by the SM sensor head.

The SSA-SM sensor head (an approximate size of 3 cm ×6 cm) was mounted on a mechanical shaker (Fig. 2) that was used to generate vibrations disturbing the sensor. A commercial PZT actuator from PhysikInstrumente (P753.2CD) served as target. This device also has a built-in capacitive feedback sensor with 2nm resolution that served as a reference sensor for the PZT target movement $D_{PZT}(t)$. It thus allowed the calculation of error between the corrected signal $D^c(t)$ and the reference motion $D_{PZT}(t)$.

Simulated and experimental tests, conducted using RLS and LMS algorithms to validate the utility of adaptive filter for the cancellation of parasitic vibrations corrupting the SM sensor output, are detailed in the following.

B. *Results of Simulated Signals*

In order to test if an adaptive filter can allow parasitic vibration cancellation in a SM vibration sensor, various simulation based cases were evaluated by using LMS and RLS algorithms, as detailed below.

First, it was simulated to test if the adaptive filter can tune itself to provide correction if the target as well as the sensor are both vibrating at two different frequencies.

Fig. 4 represents such a case where the target vibration is at f_{PZT} = 85 Hz with a peak-to-peak amplitude A_{p-p} = 5 µm while parasitic vibration disturbing the sensor is at f_s = 52 Hz again with A_{p-p} = 5 µm. The corresponding SM signal, simulated by

DOI: 10.1109/TIM.2016.2626018

employing the SM behavioral model detailed in [26] is shown in Fig. 4(a).The corrupted signal $D_{\Sigma}(t)$ is shown in Fig. 4 (b). After the convergence of the adaptive filter, corrected vibration $D^c(t)$matches very well with the reference target vibration $D_{PZT}(t)$ shown in Fig. 4 (d). The error between the corrected and reference target motion $£(t) = D_{PZT}(t) - D^c(t)$ is shown in Fig. 4 (e) which has an rms value of 4.41 nm (LMS) and 13.2nm (RLS).

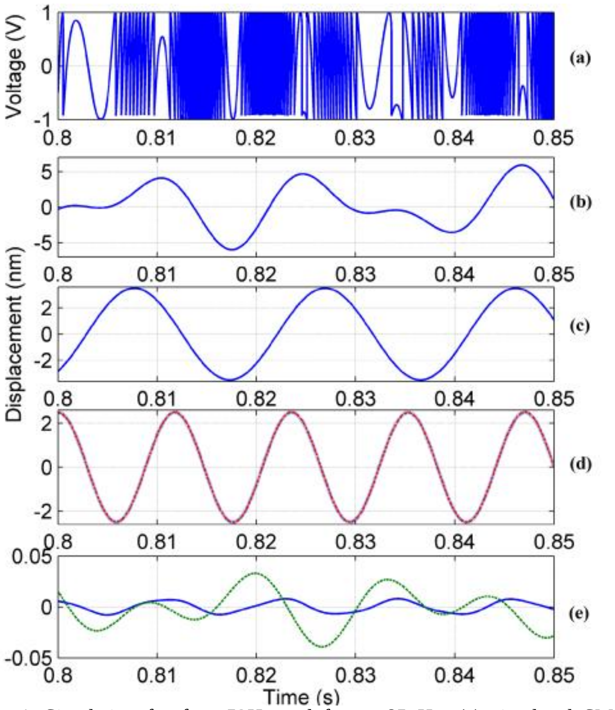

Fig. 4. Simulation for f_s = 52Hz and f_{PZT} = 85 Hz: (a) simulated SM interferometric signal, (b) corrupted vibration $D_{\Sigma}(t)$retrieved by PUM, (c) parasitic vibration $D_s(t)$, (d) corrected vibration $D^c(t)$(blue (LMS) , green (RLS)) and reference vibration $D_{PZT}(t)$ (dotted red), and (e) error $£(t)= D_{PZT}(t)- D^c(t)$ (blue (LMS), dotted green (RLS)) over 20Hz-500Hz.

Second, it was simulated to test if the adaptive filter can provide acceptable correction if multiple parasitic harmonic vibrations disturb the SM vibration sensor.

Fig. 5 represents such a case where the parasitic vibrations disturbing the SM sensor are at f_s = 61Hz-122Hz-305Hz-427Hz while the target vibration is at f_{PZT} = 81 Hz. As a consequence, the vibration retrieved through the SM signal is heavily corrupted, as seen in Fig. 5 (b). However, the corrected vibration $D^c(t)$again matches very well with $D_{PZT}(t)$shown in Fig. 5 (d) with an rms error of 8.82nm (LMS) and 12.2nm (RLS).

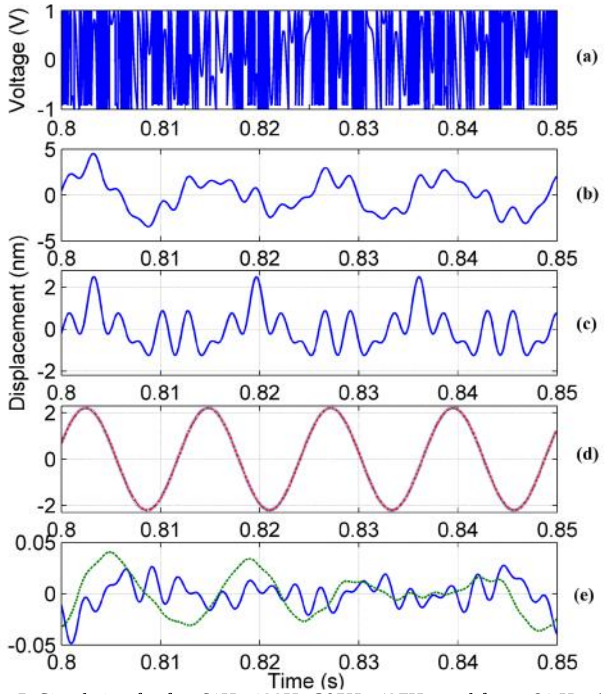

Fig. 5. Simulation for f_s = 61Hz-122Hz-305Hz-427Hz and f_{PZT} = 81 Hz: (a) simulated SM interferometric signal, (b) corrupted vibration $D_{\Sigma}(t)$ retrieved by PUM, (c) parasitic vibration $D_s(t)$, (d) corrected vibration $D^c(t)$ (blue (LMS) , green (RLS)) and reference vibration $D_{PZT}(t)$ (dotted red), and (e) error $£(t) = D_{PZT}(t) - D^c(t)$ (blue (LMS), dotted green (RLS)) over 20Hz-500Hz.

TABLE I. ADAPTIVE FILTER SPECIFICATION AND RMS ERROR RESULTS OF SIMULATED SIGNALS FOR DIFFERENT VIBRATIONS OF TARGET & SHAKER OVER (20HZ-500HZ) BANDWIDTH

Shaker (Hz)	**PZT (Hz)**	**Signal Avg Power P_{av}**	**Filter Order N**	**Conve-gence factor μ**	**LMS RMS Error (nm)**	**RLS RMS Error (nm)**
52	85	9.25	300	7e-5	4.41	13.2
92	65	5.12	350	7e-5	9.74	7.44
143	46	5.11	170	8e-4	7.97	1.89
223	131	6.25	200	9e-4	5.61	3.80
43	105	9.25	280	6e-5	5.88	7.26
123	73	7.62	360	9e-5	4.51	5.10
229	59 arb[a]	7.20	300	7e-5	8.42	3.89
61 arb[b]	81	4.12	170	4e-4	8.82	12.2
51 arb[c]	41arb[d]	4.16	700	9e-5	14.1	9.49
				mean	**7.71**	**7.14**

[a]59Hz-118Hz-295Hz-413Hz [c] 51Hz-102Hz-255Hz-357Hz

[b]61Hz-122Hz-305Hz-427Hz [d]41Hz-82Hz-205Hz-287Hz

Various other simulations were also performed (see Table I). All of these gave satisfactory results thereby validating the use of adaptive filter in the absence of pre-calibration. It may be noted that all results based on RLS algorithm, simulated as well as experimental used constant filter order N_{RLS} of 35 and adaptation factor Λ of 1. On the other hand filter order N_{LMS} and convergence factorμ of LMS algorithm were varied for each case of Table I due to reasons detailed later on in Section V.

DOI: 10.1109/TIM.2016.2626018

C. *Results of Experimental Signals*

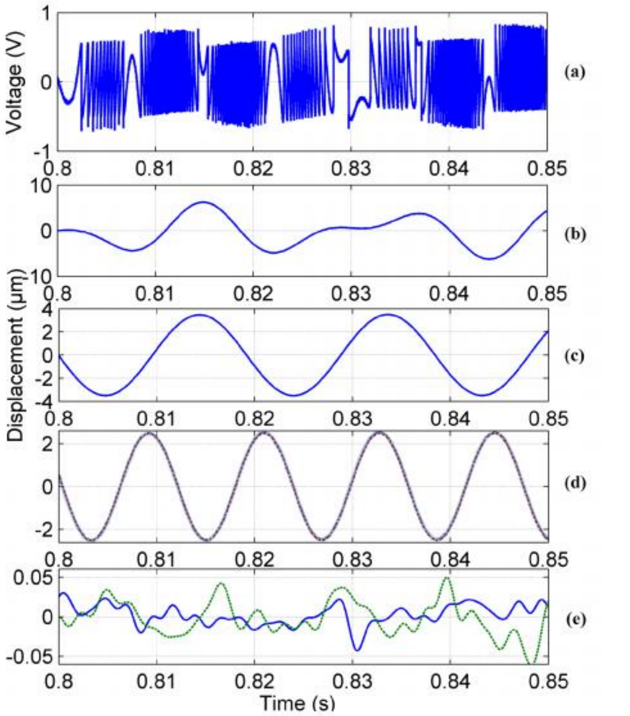

Fig. 6. Experimental signals for f_s = 52Hz and f_{PZT} = 85Hz: (a) experimental SM interferometric signal picked up by DL7140, (b) corrupted vibration $D_{\Sigma}(t)$retrieved by PUM, (c) parasitic vibration $D_s(t)$measured by SF1500 SSA, (d) corrected vibration $D^c(t)$(blue (LMS) , green (RLS)) and reference capacitive feedback sensor vibration $D_{PZT}(t)$ (dotted red), and (e) error £(t)= $D_{PZT}(t)$ - $D^c(t)$(blue (LMS), dotted green (RLS)) over 20Hz-500Hz.

Using the experimental set-up already detailed, many experimental signals were acquired to validate the principle. The experimental acquisitions are at the same frequencies as already used in the simulated signals. Thus, it would be possible to make a meaningful comparison between the simulated and experimental cases.

Therefore, first, the PZT vibration was set at f_{PZT} = 85 Hz with A_{p-p} = 5 µm while parasitic vibration disturbing the sensor is at f_s = 52 Hz with A_{p-p} = 7 µm (measured by SF1500 SSA). The corresponding experimental SM signal is shown in Fig. 6 (a) which has been unwrapped by using PUM to provide $D_{\Sigma}(t)$ shown in Fig. 6(b). In spite of the higher vibration amplitudes, the use of adaptive filter has corrected it to provide $D^c(t)$which matches very well with the reference target capacitive feedback sensor vibration $D_{PZT}(t)$ shown in Fig. 6 (d). The error £(t) = $D_{PZT}(t)$ - $D^c(t)$ is shown in Fig. 6 (e) with an rms value of 13.6 nm(LMS) and 16.9nm (RLS).

Second, an experiment was conducted for the case where the shaker is excited by 229Hz while PZT target was excited by a signal composed of 59Hz-118Hz-295Hz-413Hz (see Fig.7).In spite of the fact that this case is more complicated than the previous case but still a good correction has been achieved with an rms error of 18.2nm (LMS) and 20.5nm (RLS).

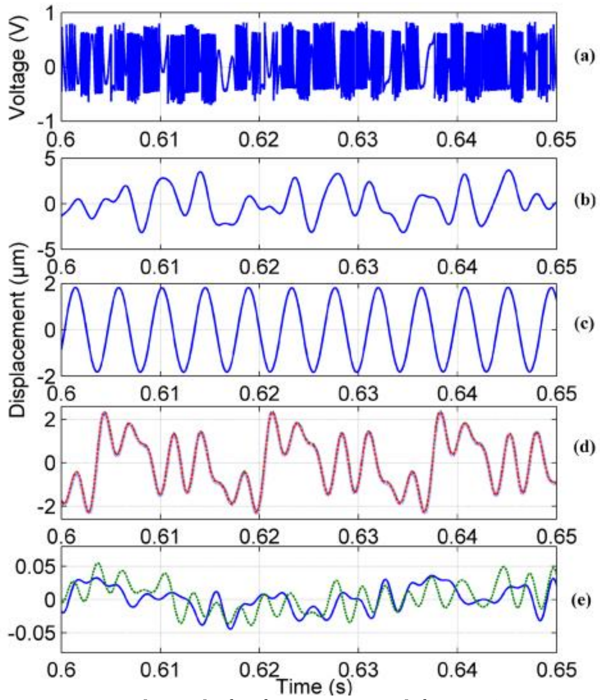

Fig.7. Experimental signals for f_s = 229Hz and f_{PZT} = 59Hz-118Hz-295Hz-413Hz : (a) experimental SM interferometric signal picked up by DL7140 (b) corrupted vibration $D_{\Sigma}(t)$retrieved by PUM, (c) parasitic vibration $D_s(t)$ measured by SF1500 SSA, (d) corrected vibration $D^c(t)$ (blue (LMS) , green (RLS)) and reference capacitive feedback sensor vibration $D_{PZT}(t)$(dotted red), and (e) error £(t) = $D_{PZT}(t)$ - $D^c(t)$ (blue (LMS), dotted green (RLS)) over 20Hz-500Hz.

Third, an experiment was conducted to see if multiple parasitic harmonic vibrations disturbing the SM vibration sensor can also be cancelled by using the proposed methods.

Fig. 8 thus shows the experimentally acquired signals for f_s = 51Hz-102Hz-255Hz-357Hz and f_{PZT} = 41Hz-82Hz-205Hz-287Hz. In spite of multiple mechanical vibrations disturbing the SM sensor, a good recovery of true target vibration has been achieved, as seen in Fig. 8 (e) with an rms error of 28.5 nm(LMS) and 24.2nm (RLS).The frequency spectra of Fig. 9 show corrections of 20.3dB (28.4dB), 24.2dB (21.3dB), 18.3dB (19.1dB), and 20.1dB (18.7dB)at51Hz, 102Hz, 255Hz, and 357Hz respectively using LMS algorithm (RLS algorithm).

Finally, the results of these and all other experimental cases are presented in Table II.

V. Discussion

A. *Performance of LMS based Adaptive Sensor*

A comparison of Table I and Table II indicates that the error values are expectedly higher for experimental signals as compared to simulated signals due to the addition of different error sources, such as the imprecision of SM displacement retrieval method, the imprecision of the SSA measuring the parasitic movement, the noise of electronic circuits and data acquisition path etc. Similarly, the filter orders of LMS algorithm are generally higher for the experimental signal

DOI: 10.1109/TIM.2016.2626018

acquisitions as compared to the filter orders LMS algorithm for the simulated signals for the same reasons.

It can be seen from Table I and Table II that LMS based optimal correction is only achieved when its parameters such as N and μ are adjusted as function of input signal's power P_{av} as per (6).

In order to achieve optimal correction results, note that the filter order for any given signal was kept on increasing so long as final error kept on reducing while maintaining a stable convergence of the algorithms. Thus, the highest filter order leading to the lowest errors are reported. For such a filter order, the final error of the adaptive system reaches the noise floor. Subsequently, any further increase in filter order would not lead to improvement in the final error results.

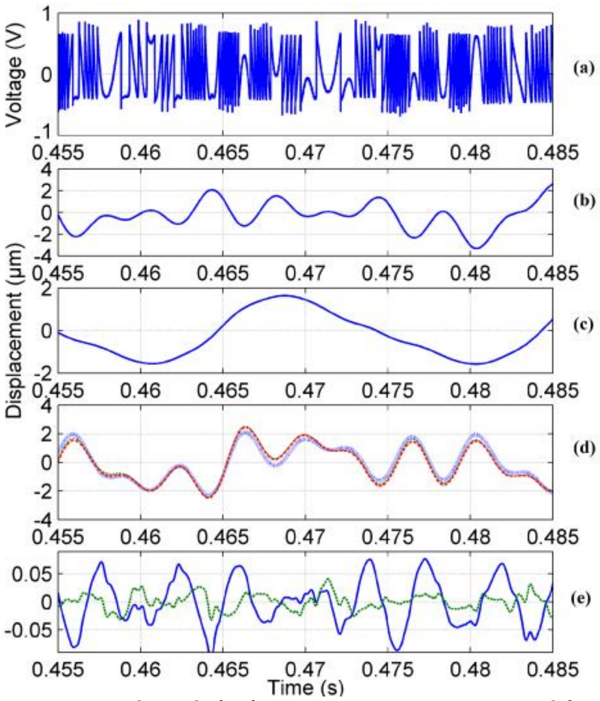

Fig. 8.Experimental signals for f_s = 51Hz-102Hz-255Hz-357Hz and f_{PZT} = 41Hz-82Hz-205Hz-287Hz: (a) experimental SM interferometric signal picked up by DL7140, (b) corrupted vibration $D_{\Sigma}(t)$retrieved by PUM, (c) parasitic vibration $D_s(t)$measured by SF1500 SSA, (d) corrected vibration $D^c(t)$ (blue (LMS) , green (RLS)) and reference capacitive feedback sensor vibration D_{PZT}(dotted red), and (e) error £ (t)= D_{PZT} (t)- $D^c(t)$ (blue (LMS), dotted green (RLS)) over 20Hz-500Hz.

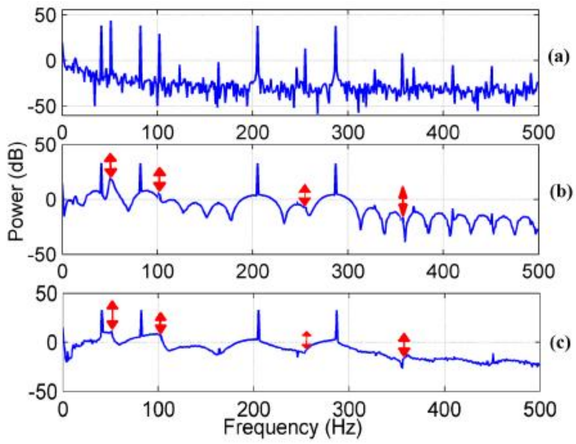

Fig.9.Experimental signals for f_s = 51Hz-102Hz-255Hz-357Hz and f_{PZT} = 41Hz-82Hz-205Hz-287Hz: (a) frequency spectrum of corrupted vibration $D_{\Sigma}(t)$, (b) LMS and (c) RLS algorithm based frequency spectrum of corrected vibration $D^c(t)$indicating an improvement corrections of 20.3dB (28.4dB), 24.2dB (21.3dB), 18.3dB (19.1dB), and 20.1dB (18.7dB) at 51Hz, 102Hz, 255Hz, and 357Hz.

TABLE II. ADAPTIVE FILTER SPECIFICATION AND RMS ERROR RESULTS FOR EXPERIMENTAL SIGNALS OF DIFFERENT VIBRATIONS OF TARGET & SHAKER OVER (20HZ-500HZ) BANDWIDTH

Sha-ker (Hz)	PZT (Hz)	Signal Avg Power P_{av}	Filter order N_{LMS}	Conve-gence factor μ	LMS RMS Error (nm)	RLS RMS Error (nm)	Exemp-lar [14] Error (nm)
52	85	10.37	390	6e-5	13.6	16.9	31.9
92	65	5.785	400	4e-5	12.5	15.8	24.9
143	46	5.993	120	3e-4	17.1	17.9	17.0
223	131	6.384	260	9e-4	14.7	16.7	17.4
43	105	6.209	380	4e-5	13.7	14.8	22.0
123	73	7.936	120	2e-4	11.5	16.5	28.1
229	59 [a]	3.411	530	7e-5	18.2	20.5	16.9
61 [b]	81	7.254	450	7e-5	41.7	38.7	31.8
41 [c]	51 [d]	3.092	500	4e-5	28.5	24.2	32.1
--	--	--	--	**mean**	**19.1**	**20.22**	**24.7**

[a].59Hz-118Hz-295Hz-413Hz [c] 51Hz-102Hz-255Hz-357Hz
[b].61Hz-122Hz-305Hz-427Hz [d].41Hz-82Hz-205Hz-287Hz

An analysis of tabulated results also brings forth the relationship between filter order, convergence factor, and input signal power for LMS based adaptive FIR filter. It can be seen in Table II that higher filter orders result in smaller convergence factors which cause slower convergence. On the other hand, average power of signal also affects the convergence factor. For example, 143Hz-46Hz case has larger convergence factor as compared to 123Hz-73Hz case even though the filter order is the same. This is due to the difference in their respective average powers. Therefore, it is both filter order and average signal power that determine stable convergence of LMS adaptive filter.

B. Performance of RLS based Adaptive Sensor

In the case of RLS algorithm based SSA-SM sensor, parasitic vibration correction is independent of parameters adjustment. Thus, its filter order N_{RLS} and adaptation factor Λ can be kept constant for all the cases. This makes it suited for

DOI: 10.1109/TIM.2016.2626018

practical, real-time experimental measurements scenarios as it requires no intervention in terms of its parameters. As a result, the SSA-SM sensor using this adaptive filter is then able to work autonomously while delivering comparable measurements precision at even better convergence rates.

C. Comparison of LMS and RLS based Systems / Sensors

A comparison of rate of convergence of LMS and RLS algorithms is shown in Fig. 10 which uses the experimental data of f_s=92Hz and f_{PZT}=65Hz case. When the performance of RLS is compared with that of LMS for the same filter of 80 then it is seen that RLS achieves convergence at a better rate (e.g. 173 iteration for RLS and 1100 iterations for LMS for filter order of 80, leading to an rms error of 14.7nm and 28.9nm respectively) Focusing only on LMS algorithm, the impact of choosing higher filter order (leading to smaller error) on the convergence time (causing slower convergence) of LMS algorithm based adaptive filter is also depicted in Fig.10. Here, the filter roughly took 3700 iterations to reach convergence resulting in final rms error of 12.5 nm for N = 400.

Thus, the use of RLS algorithm has resulted in achieving convergence after 17.3 ms. For an input sampling rate of 10 000 samples per second, equating to a total computational time per iteration of 0.1 ms in the context of a real-time system, the adaptive SSA–SM system achieves convergence in 17.3 ms for the RLS algorithm for the above-mentioned case. Even in the worst case (i.e., the use of LMS algorithm with N_{LMS} = 400), convergence is achieved after 0.37 s, thereby underlining the performance of the adaptive filter scheme.

Regarding measurement precision, the results of the RLS and LMS algorithms are almost comparable to each other with minor differences (see Tables I and II). Yet, we can claim that the performance of the RLS algorithm is better than that of the LMS algorithm because the filter order of the RLS algorithm is very small compared with that of the LMS algorithm, and it achieves convergence at a faster rate without any external intervention. However, this superior performance of RLS is attained at the expense of a large increase in computational complexity, as detailed below.

The complexity level of the RLS algorithm requires a total of $4N^2+4N+2$ multiplications (division counted as multiplication) while LMS algorithm requires $2N+1$ multiplications only, where N is filter's order [27].

The advantage of LMS algorithm is its simple structure requiring only vector operations as seen in (4-5). The RLS algorithm structure, on other hand, is much more complex, requiring the calculation and updating of input auto-correlation matrix as seen in (7-9).

D. Comparison with pre-calibration based sensor / system.

Finally, a comparison can be made between the performance of the adaptive filter based instrument and that of the previously proposed pre-calibration based instrument [12]. Note that the last column of Table II cites the published results of Zabit et al. [14] and that the authors have used the same experimental signal acquisitions for the present study. It can be seen that the proposed method enables improved mean rms error of 19.1nm and 20.2nm for LMS and RLS respectively as compared to pre-calibration based results having mean rms error of 24.7nm.

It thus highlights the performance of adaptive filter based instrument which not only removes the problems involved in the design of pre-calibration based instrument but also leads to better correction results. This improved performance of the adaptive filter based instrument can be explained by the absence of errors caused by imprecision either in the extraction of phase and gain parameters or in the design of equalization filter. Furthermore, by its very nature, at any given time, the adaptive filter is able to concentrate its attenuation over a very small set of frequencies whereas the equalization filter provides equally weighted attenuation over the whole operating bandwidth of the instrument. Thus, except for the cases where $f_s=f_{PZT}$ which cannot be solved by an adaptive filter, the proposed method not only helps to avoid the difficulties associated with pre-calibration but also provides on average better measurement precision.

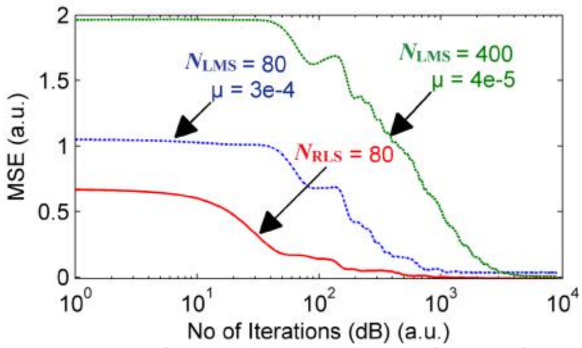

Fig.10. Evolution of mean square error (MSE) as function of number of iterations needed by the adaptive LMS and RLS algorithms for the experimental case of f_s =92Hz and f_{PZT} = 65Hz.

Finally, the simple and computationally light LMS based adaptive filter is only suitable for a real-time system implementation without external intervention if additional processing is incorporated in it to adjust filter order and convergence factor as a function of input signal's power. Such an obstacle is completely removed if the RLS algorithm is deployed as it requires no external intervention and works optimally in an autonomous manner.

VI. CONCLUSION

In this paper, it has been demonstrated that the use of adaptive filters can allow us to design a laser vibration sensor that can provide correct measurements even when the sensor itself is disturbed by extraneous parasitic motion. The use of adaptive filter with an accelerometer coupled Self-Mixing laser instrument thus potentially allows sensing (without needing any pre-calibration) in hostile/embedded environment where such extraneous movements which mechanically disturb the sensor cannot be avoided.

For this purpose, LMS algorithm was used with a transversal FIR adaptive filter structure. It was chosen over other advanced algorithms as it requires less computational

DOI: 10.1109/TIM.2016.2626018

power and memory while achieving the task of parasitic vibration cancellation in a stable manner. However, the main drawback of LMS algorithm is the difficulty of predefining the value of learning rate or convergence factor μ that ensures the adaptive filter's stability in case of variations in input signal power, as seen in (6).

For these reasons, RLS algorithm would be then be preferable choice for a real-time adaptive SSA-SM sensor as its filter parameters are independent of input signal's characteristics. Furthermore it has superior performance as compared to LMS algorithm in terms of faster convergence, the rms error of both algorithms are also comparable, so one can safely say RLS is the better choice but at the cost of additional computational complexity.

The main advantage of the LMS filter is the comparative simplicity of the algorithm. However, for signals with a large eigenvalue spread, the LMS has an unstable and slow convergence rate [25]. In addition to this non-stationary signals with high rate of change with time, the LMS can be an unsuitable adaptation solution, on the other hand, RLS method, with its better convergence rate and less sensitivity to the eigenvalue spread, becomes a more attractive alternative [25].

For the different monotone experimental parasitic vibration cases (tabulated in Table II), the proposed methods has resulted in mean rms error in final displacement correction of better than 15 nm. It is a noteworthy result as it is a precision value similar to what can be obtained with a SM sensor by using PUM in the absence of parasitic vibrations. That is, for monotone parasitic vibrations, the adaptive SSA-SM system has provided almost ideal correction.

REFERENCES

[1] S. Donati, "Developing self-mixing interferometry for instrumentation and measurements", *Laser & Photon. Rev*., 6: 393417, May 2012.

[2] T. Taimre, M. Nikolić, K. Bertling, Y. L. Lim, T. Bosch, and A. D. Rakić, "Laser feedback interferometry: a tutorial on the self-mixing effect for coherent sensing," *Adv. Opt. Photon*. 7, 570-631 (2015).

[3] Scalise, L.; Yanguang Yu; Giuliani, G.; Plantier, Guy; Bosch, T., "Self-mixing laser diode velocimetry: application to vibration and velocity measurement," *Instrumentation and Measurement, IEEE Transactions on*, vol.53, no.1, pp. 223-232, Feb. 2004.

[4] Y. Fan, Y. Yu, J. Xi, and J. F. Chicharo, "Improving the measurement performance for a self-mixing interferometry-based displacement sensing system," *Appl. Opt*. 50, 5064-5072 (2011).

[5] Magnani, A; Pesatori, A; Norgia, M., "Real-Time Self-Mixing Interferometer for Long Distances," *Instrumentation and Measurement, IEEE Transactions on*, vol.63, no.7, pp.1804-1809, July. 2014.

[6] Norgia, M.; Giuliani, G.; Donati, S., "Absolute Distance Measurement with Improved Accuracy Using Laser Diode Self-Mixing Interferometry in a Closed Loop," *Instrumentation and Measurement, IEEE Transactions on*, vol.56, no.5, pp. 1894-1900, Oct. 2007.

[7] Plantier, Guy; Servagent, N.; Bosch, T.; Sourice, A, "Real-time tracking of time-varying velocity using a self-mixing laser diode," *Instrumentation and Measurement, IEEE Transactions on*, vol.53, no.1, pp. 109-115, Feb. 2004.

[8] O. D. Bernal, U. Zabit, and T. Bosch, "Study of Laser Feedback Phase under Self-Mixing leading to Improved Phase Unwrapping for Vibration Sensing", *IEEE Sensors Journal*, vol.13, no.12, pp. 4962-4971, 2013.

[9] Ozdemir, S.K.; Ohno, I; Shinohara, S., "A Comparative Study for the Assessment on Blood Flow Measurement Using Self-Mixing Laser Speckle Interferometer," *Instrumentation and Measurement, IEEE Transactions on*, vol.57, no.2, pp. 355-363, Feb. 2008.

[10] M. Wang and G. Lai, "Self-mixing microscopic interferometer for the measurement of microprofile", *Optics Communications, vol.* 238, no 4–6, pp.237–244, August.2004.

[11] Vogel, F.; Toulouse, B., "A low-cost medium-resolution rangefinder based on the self-mixing effect in a VCSEL," *Instrumentation and Measurement, IEEE Transactions on*, vol.54, no. 1, pp.428-431, Feb. 2005.

[12] Donati, S.; Norgia, M., "Self-Mixing Interferometry for Biomedical Signals Sensing," *Selected Topics in Quantum Electronics, IEEE Journal of*, vol.20, no.2, pp.104-111, March-April. 2014.

[13] Milesi, I; Norgia, M.; Pompilio, P.P.; Svelto, C.; Dellaca, R.L., "Measurement of Local Chest Wall Displacement by a Custom Self-Mixing Laser Interferometer," *Instrumentation and Measurement, IEEE Transactions on*, vol.60, no.8, pp. 2894-2901, Aug. 2011.

[14] Zabit, U.; Bernal, O.D.; Bosch, T., "Design and Analysis of an Embedded Accelerometer Coupled Self-Mixing Laser Displacement Sensor," *Sensors Journal, IEEE*, vol.13, no.6, pp.2200-2207, June. 2013.

[15] Zabit, U.; Bernal, O.D.; Chamorro-Coloma, A; Bosch, T., "Real-time accelerometer coupled Self-Mixing laser displacement sensor for embedded applications," *Sensors, 2012 IEEE*, vol., no., pp.1,4, 28-31 Oct. 2012.

[16] R. Lang and K. Kobayashi, "External optical feedback effects on semiconductor injection laser properties," *Quantum Electronics, IEEE Journal*of 16, 347-355 (1980).

[17] C. Henry, "Theory of the linewidth of semiconductor lasers," *Quantum Electronics, IEEE Journal* of 18, 259-264 (1982).

[18] Y. Yu, G. Giuliani, and S. Donati, "Measurement of the linewidth enhancement factor of semiconductor lasers based on the optical feedback self-mixing effect," *Photonics Technology Letters, IEEE* 16, 990-992 (2004).

[19] G. A. Acket, D. Lenstra, A. Den Boef, and B. Verbeek, "The influence of feedback intensity on longitudinal mode properties and optical noise in index-guided semiconductor lasers," *Quantum Electronics, IEEE Journal* of 20, 1163-1169 (1984).

[20] T. Taimre and A. D. Raki, "On the nature of Acket's characteristic parameter C in semiconductor lasers," *Appl. Optics* 53, 1001-1006 (2014).

[21] Y. Yu, J. Xi, J. F. Chicharo, and T. M. Bosch, "Optical Feedback Self-Mixing Interferometry With a Large Feedback Factor C: Behavior Studies," *Quantum Electronics, IEEE Journal* of 45, 840-848 (2009).

[22] Bernal, O.D.; Zabit, U.; Bosch, T, "Classification of laser SMI signal under moderate feedback," *Applied Optics*, vol. 53, no. 4, pp. 702-708, (2014).

[23] C. Bes, G. Plantier and T. Bosch, "Displacement measurements using a self-mixing laser diode under moderate feedback", *Instrumentation and Measurement, IEEE Transactions on*, vol. 55, no.4, pp.1101-1105,Aug.2006.

[24] Paulo S.R. Diniz, Adaptive Filtering Algorithms and Practical Implementation Third Edition Springer.ISBN: 978-0-387-31274-3

[25] Saeed V. Vaseghic, Advanced Digital Signal Processing and Noise Reduction Fourth Edition 2008 John Wiley & Sons, Ltd. ISBN: 978-0-470-75406-1

[26] G. Plantier, C. Bes, and T. Bosch, "Behavioral Model of a Self-Mixing Laser Diode Sensor," *Quantum Electronics, IEEE Journal* of 41, 1157-1167 (2005).

[27] Ben Allen, M. Ghavami, Adaptive Array Systems fundamental and its application 2005 John Wiley & Sons, Ltd. ISBN: 978-0-470-86189-9

DOI: 10.1109/TIM.2016.2626018